

Reduction of mosaic spread using iridium interlayers: A route to improved oxide heteroepitaxy on silicon

S. Gsell, M. Fischer, R. Brescia, M. Schreck, P. Huber, F. Bayer, B. Stritzker, and D. G. Schlom

Citation: [Applied Physics Letters](#) **91**, 061501 (2007); doi: 10.1063/1.2768003

View online: <http://dx.doi.org/10.1063/1.2768003>

View Table of Contents: <http://scitation.aip.org/content/aip/journal/apl/91/6?ver=pdfcov>

Published by the [AIP Publishing](#)

Articles you may be interested in

[High optical and switching performance electrochromic devices based on a zinc oxide nanowire with poly\(methyl methacrylate\) gel electrolytes](#)

Appl. Phys. Lett. **105**, 193301 (2014); 10.1063/1.4901443

[Controlled epitaxial integration of polar ZnO\(0001\) with Si\(001\)](#)

Appl. Phys. Lett. **102**, 101602 (2013); 10.1063/1.4795126

[Growth of biepitaxial zinc oxide thin films on silicon \(100\) using yttria-stabilized zirconia buffer layer](#)

Appl. Phys. Lett. **93**, 251905 (2008); 10.1063/1.3050529

[Low-voltage-driven top-gate ZnO thin-film transistors with polymer/high- k oxide double-layer dielectric](#)

Appl. Phys. Lett. **89**, 133507 (2006); 10.1063/1.2357559

[A route to diamond wafers by epitaxial deposition on silicon via iridium/yttria-stabilized zirconia buffer layers](#)

Appl. Phys. Lett. **84**, 4541 (2004); 10.1063/1.1758780

An advertisement for Oxford Instruments Atomic Force Microscopy (AFM) systems. The background is dark blue with a light blue wavy pattern. On the left, there is a black mobile phone and a white desktop computer. In the center, there is a white AFM instrument. Text on the left reads: 'You don't still use this cell phone or this computer'. Text in the center reads: 'Why are you still using an AFM designed in the 80's?'. Text on the right reads: 'It is time to upgrade your AFM', 'Minimum \$20,000 trade-in discount for purchases before August 31st', and 'Asylum Research is today's technology leader in AFM'. At the bottom right, there is the Oxford Instruments logo and the tagline 'The Business of Science®'. The email address 'dropmyoldAFM@oxinst.com' is also present.

Reduction of mosaic spread using iridium interlayers: A route to improved oxide heteroepitaxy on silicon

S. Gsell, M. Fischer, R. Brescia, M. Schreck,^{a)} P. Huber, F. Bayer, and B. Stritzker
Institut für Physik, Universität Augsburg, D-86135 Augsburg, Germany

D. G. Schlom

Department of Materials Science and Engineering, The Pennsylvania State University, University Park, Pennsylvania 16802-5005

(Received 23 May 2007; accepted 10 July 2007; published online 6 August 2007)

Using epitaxial SrTiO₃ and yttria-stabilized zirconia (YSZ) buffer layers deposited on silicon as a starting point, epitaxial iridium layers were grown by electron-beam evaporation using a two-step growth process with an extremely low initial deposition rate. The iridium layers had in-plane (twist) and out-of-plane (tilt) full widths at half maximum as narrow as 0.08° and 0.15°, respectively, up to an order of magnitude narrower than the underlying SrTiO₃ and YSZ layers. SrTiO₃ and ZnO films grown on the iridium showed significantly narrower twist and tilt values than without the iridium interlayer, demonstrating a route to improved oxide heteroepitaxy on silicon. © 2007 American Institute of Physics. [DOI: 10.1063/1.2768003]

Silicon is an attractive substrate for the heteroepitaxial growth of a variety of functional oxides. To avoid reaction between the functional oxide and the underlying silicon, an epitaxial oxide buffer layer that is stable in contact with silicon¹ is typically introduced, forming a functional oxide/oxide buffer/silicon heterostructure. Such epitaxial buffer layers include MgO,² SrO,³ BaO,⁴ Y₂O₃,⁵ CeO₂,⁶ ZrO₂,⁷ Y₂O₃-ZrO₂,^{5,8} and Al₂O₃.⁹ Via these buffer layers, a multitude of functional oxides, including high-temperature superconductors⁵ and ferroelectrics,⁸ have been epitaxially integrated with silicon.

Unfortunately, the in-plane and out-of-plane epitaxial alignments (mosaic spreads) of epitaxial oxides on silicon as deduced from x-ray diffraction (XRD) rocking curves and azimuthal scans are still significantly higher¹⁰ than that of state-of-the-art semiconductor heterostructures.^{11,12} Further reduction of the mosaic spread and simpler processes for the heteroepitaxial integration of high quality functional oxides with silicon are therefore desired.

In the present work we show that the epitaxial iridium films with very low mosaic spread can be grown on epitaxial oxide buffer layers on silicon. When epitaxial oxides are in turn grown on these iridium interlayers, the result is an oxide layer with a significantly reduced mosaic spread. This provides a new route for the realization of higher quality epitaxial oxide layers on silicon.

Two different techniques, molecular-beam epitaxy (MBE) and pulsed-laser deposition (PLD), were applied for the preparation of the oxide layers in this work. The heteroepitaxial SrTiO₃ buffer layers on silicon were grown by MBE. The growth process involves the formation of a strontium silicide layer on a cleaned and 2×1 reconstructed Si(001) surface, the consecutive deposition of SrO and TiO₂ which are transformed into SrTiO₃ in a topotactic reaction, and finally the epitaxial SrTiO₃ growth by depositing alternating monolayers of TiO₂ and SrO. Details on the process parameters are given in Ref. 13.

YSZ films on silicon and the SrTiO₃ layers on iridium were prepared by PLD with a KrF excimer laser (pulse duration: 25 ns, pulse energy: 700–850 mJ) using cylindrical targets. The stoichiometry of the cubic YSZ target was (YO_{1.5})_{0.21}(ZrO₂)_{0.79}. Ablation was done at substrate temperatures between 750 and 850 °C in an oxygen background pressure of 5×10⁻⁴ mbar for YSZ and 7×10⁻⁵ mbar for SrTiO₃. During YSZ growth the first 300 pulses were performed in high vacuum to remove the amorphous silicon oxide. The iridium layers were deposited by electron-beam evaporation at a substrate temperature of 650 °C in high vacuum (10⁻⁶ mbar).

Figure 1 shows θ -2 θ XRD scans of two 150-nm-thick iridium films deposited on a MBE-grown SrTiO₃/Si(001) substrate. In Fig. 1(a) the iridium was grown with a deposition rate of 0.05 nm/s. Although this rate yielded (001)-oriented epitaxial iridium films with low mosaic spread on SrTiO₃ single crystals,^{14,15} the XRD pattern of the present Ir/SrTiO₃/Si stack is dominated by a strong 111 Ir peak with only a minor fraction (~1%) of (001)-oriented epitaxial iridium. For the iridium layer in Fig. 1(b) a nucleation step with a strongly reduced deposition rate of 0.002 nm/s was applied for the first 20 nm. The XRD pattern contains only the 002 peak of epitaxial iridium with negligible (<0.1%) signal from other iridium-related Bragg reflections.

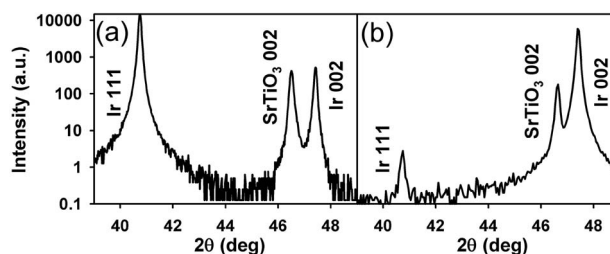


FIG. 1. θ -2 θ scans of two 150-nm-thick iridium films deposited on an MBE-grown SrTiO₃ buffer layer on Si(001). Iridium deposition rate: (a) 0.05 nm/s and (b) 0.002 nm/s for the first 20 nm. Intensity ratio I(Ir 200)/I(Ir 111): (a) 0.03 and (b) 2100.

^{a)} Author to whom correspondence should be addressed; electronic mail: matthias.schreck@physik.uni-augsburg.de

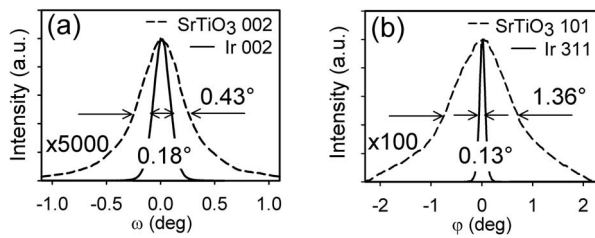


FIG. 2. Rocking curves and azimuthal scans of the iridium overlayer and the SrTiO₃ buffer layer of the Ir/SrTiO₃/Si(001) epitaxial heterostructure (sample 2 in Table I).

Figures 2(a) and 2(b) show high resolution tilt and twist measurements for an iridium layer grown on SrTiO₃/Si(001) using the low growth rate nucleation step described above. The rocking curves and azimuthal scans for the iridium film and the SrTiO₃ buffer layer differ dramatically. Surprisingly, the full width at half maximum (FWHM) of the overlying iridium layer is much narrower than that of the underlying oxide buffer layer by factors of 2.5 and 10 for tilt and twist, respectively.

To test whether this behavior can also be observed for other oxides and growth planes, iridium was deposited on YSZ/Si(001) and YSZ/Si(111) buffer layers. The starting YSZ/Si buffer layers have tilt and twist FWHM comparable to state-of-the-art values reported in the literature for buffer layers of similar thickness.^{5,16} The results, summarized in Table I, show that a reduction in mosaic spread by an order of magnitude for tilt and twist can be achieved [see Ir/YSZ/Si(111)]. Tilt and twist FWHMs as narrow as 0.15° and 0.08°, respectively, were found for the iridium layers on YSZ/Si(001).

The microstructure and the interfaces of several heterostructures were studied by transmission electron microscopy (TEM). Figure 3 shows a cross-sectional TEM image of an Ir/YSZ/Si(001) sample with an iridium layer thickness of only 20 nm. The crystalline YSZ film is separated from the silicon substrate by a 3 nm thick amorphous silicon oxide layer. In contrast, the Ir/YSZ interface is crystalline over the whole range. The dislocation density in the iridium layer ($\sim 10^{11}$ cm⁻²) is roughly an order of magnitude

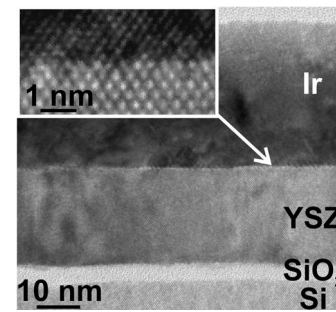


FIG. 3. Cross-sectional TEM image of an Ir(20 nm)/YSZ/Si(001) sample taken along the [110] zone axis.

lower than in the YSZ layer ($\sim 10^{12}$ cm⁻²). Thus, starting directly from the interface the crystalline quality of the iridium film is significantly higher than in the underlying oxide.

Iridium layers with low mosaic spread have been grown on 4 in. diam YSZ/Si wafers. Their suitability for the heteroepitaxial growth of single crystal diamond layers has recently been realized.¹⁷ Moreover, several properties of iridium led us to believe that the low in-plane and out-of-plane mosaic spreads of an epitaxial iridium interlayer might dramatically improve the mosaic spread of epitaxial oxide films grown on top of it. As compared to other elements of the platinum group, iridium has a high affinity to oxygen. This affinity in connection with its high melting point provides a strongly modulated surface potential necessary for the epitaxial alignment of the overlying film. The ability to limit the oxidation of iridium to its surface preserves its narrow mosaic spread and enables it to template an overlying epitaxial oxide. These rather unique properties of iridium motivated us to assess the ability of an iridium interlayer with excellent in-plane and out-of-plane epitaxial alignments to improve the mosaic spread of epitaxial oxide films grown on it. As we show below, it does indeed work for this purpose.

SrTiO₃ was grown on an Ir/SrTiO₃/Si(001) sample, where part of the MBE-grown SrTiO₃ buffer layer was not covered by the iridium interlayer to allow for a direct comparison with homoepitaxial growth (samples 6 and 7 in Table I). Figure 4(a) contrasts the mosaic spread of the starting

TABLE I. Mosaic spread (FWHM values) for the different epitaxial heterostructures discussed. The angular resolution of the used XRD setup (Ref. 17) was better than 0.05°. The twist values were deduced from azimuthal scans under consideration of the broadening contribution due to the tilt (Ref. 21). In systems 1–8 all layers besides SrTiO₃ on Si(001) (rotated by 45°, see Ref. 13) and YSZ on Si(111) (rotation by 60°) grow in a cube-on-cube registry. Sample 9: ZnO(0001)[100]||Ir(111)[1 $\bar{1}$ 0]||YSZ(111)[1 $\bar{1}$ 0]||Si(111)[10 $\bar{1}$]; sample 10: ZnO(0001)[100]||YSZ(111)[1 $\bar{1}$ 0]||Si(111)[10 $\bar{1}$].

Sample	Multilayer system	Oxide buffer layer (SrTiO ₃ or YSZ)			Ir layer			Functional top layer (SrTiO ₃ or ZnO)		
		Thickness (nm)	Tilt (deg)	Twist (deg)	Thickness (nm)	Tilt (deg)	Twist (deg)	Thickness (nm)	Tilt (deg)	Twist (deg)
1	Ir/SrTiO ₃ /Si(001)	100	0.58	1.16	150	0.30	0.33
2	Ir/SrTiO ₃ /Si(001)	10	0.43	1.29	150	0.18	0.12
3	Ir/YSZ/Si(001)	40	1.16	0.82	150	0.15	0.08
4	Ir/YSZ/Si(111)	50	2.77	1.94	150	0.31	0.23
6	SrTiO ₃ /Ir/SrTiO ₃ /Si(001)	20	1.40	1.40	150	0.30	0.43	50	0.74	1.00
7	SrTiO ₃ /SrTiO ₃ /Si(001)	20	1.40	1.40	50	1.15	1.38
8	SrTiO ₃ /Ir/YSZ/Si(001)	20	1.75	1.35	150	0.15	0.15	50	0.44	0.40
9	ZnO/Ir/YSZ/Si(111)	40	1.02	1.33	150	0.26	0.29	70	0.39	0.58
10	ZnO/YSZ/Si(111)	40	0.89	0.90	70	1.00	0.93

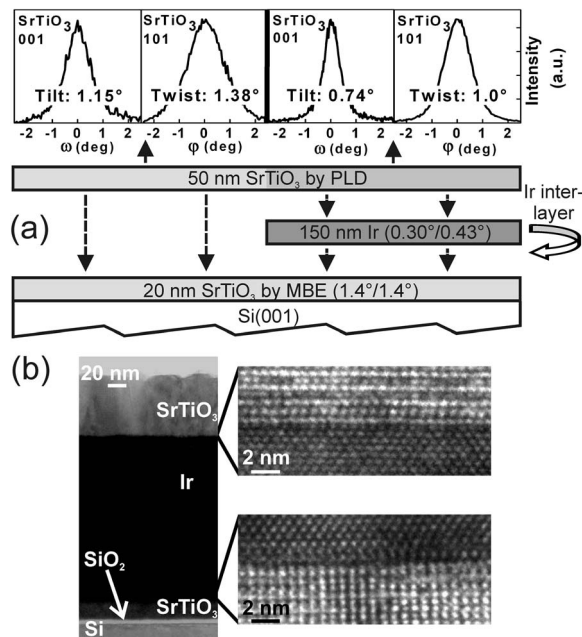


FIG. 4. (a) Mosaic spread FWHM of a MBE-grown SrTiO₃ buffer layer and a PLD-grown SrTiO₃ overlayer. On the left half of the sample the SrTiO₃ overlayer was deposited directly on top of the SrTiO₃ buffer layer. On the right half, the SrTiO₃ overlayer was deposited on a 150 nm thick epitaxial iridium interlayer. (b) TEM images of the SrTiO₃/Ir/SrTiO₃/Si(001) epitaxial heterostructure (sample 6) taken along the [110] zone axis.

MBE-grown SrTiO₃ buffer layer with the SrTiO₃ overlayer that was simultaneously deposited on the bare SrTiO₃/Si as well as on Ir/SrTiO₃/Si. The FWHMs of the SrTiO₃ layer on top of the iridium interlayer are significantly narrower than both the starting SrTiO₃ buffer layer as well as the overgrown SrTiO₃ layer that did not have the iridium interlayer beneath it. Thus, not only can oxides grow epitaxially on iridium but also the insertion of an iridium interlayer can significantly improve the mosaic spread of the overgrown epitaxial oxide layer. We also prepared SrTiO₃/Ir/YSZ/Si(001) multilayers (sample 8 in Table I), which combine the reduction in mosaic spread of the iridium interlayer with the ease of preparation of the YSZ buffer layers on silicon. The resulting SrTiO₃ overlayer had tilt and twist FWHMs of 0.4°.

As an additional example, we studied the epitaxial overgrowth of ZnO films on YSZ/Si(111) buffer layers with and without the iridium interlayer. The results (samples 9 and 10 in Table I) were quite similar: the tilt and twist of the ZnO layer on top of the iridium interlayer are significantly narrower than both the starting YSZ buffer layer as well as the overgrown ZnO layer that did not have the iridium interlayer beneath it. Using this iridium interlayer approach oriented ZnO nanopillars have also been grown.¹⁸

In summary, we have shown that epitaxial iridium layers with extremely narrow mosaic spread (FWHM < 0.1°) can be deposited on epitaxial oxide buffer layers with relatively broad mosaic spread on silicon. The strongest effect was observed for iridium on YSZ, a material pair with a lattice misfit of 25%. In most material systems misorientation of a buffer layer strongly deteriorates the crystalline quality in the subsequent layer on top. Iridium exhibits the unusual ability to form a single crystal in spite of a high density of defects in the underlying buffer layer and a huge lattice misfit. The

specific material properties of iridium and its growth mode can help to explain this effect. Iridium¹⁵ and other metals¹⁹ start in an island growth mode at the high temperatures and low deposition rates, which are required to achieve epitaxial orientation. The transition from islands to an agglomerated film can be described by the liquidlike-coalescence mechanism.²⁰ This process involves surface diffusion and rearrangement of the islands. It is most effective for layer materials with low anisotropy, high coordination, close packing, and orientation-independent bonding.²⁰ Metals are model systems with these properties. A detailed texture analysis of the first stages of iridium growth on YSZ buffer layers on silicon shows that the coalescence of the metal islands is accompanied by a realignment of the impinging islands towards an intermediate orientation, which elucidates the pronounced texture improvement. These highly oriented iridium films can serve as epitaxial templates for oxide overgrowth, leading to dramatic improvements in the crystalline quality of functional oxides on silicon.

The authors gratefully acknowledge support of this work by the AMU Augsburg and by the European community within the network DRIVE to the author R.B. (MRTN-CT-2004-512224) and within the STREP project NANOMESH to the author S.G. (NMP4-CT-2004-013817).

¹K. J. Hubbard and D. G. Schlom, *J. Mater. Res.* **11**, 2757 (1996).

²D. K. Fork, F. A. Ponce, J. C. Tramontana, and T. H. Geballe, *Appl. Phys. Lett.* **58**, 2294 (1991).

³Y. Kado and Y. Arita, *J. Appl. Phys.* **61**, 2398 (1987).

⁴R. A. McKee, F. J. Walker, J. R. Conner, E. D. Specht, and D. E. Zelmon, *Appl. Phys. Lett.* **59**, 782 (1991).

⁵Th. Matthée, J. Wecker, H. Behner, G. Friedl, O. Eibl, and K. Samwer, *Appl. Phys. Lett.* **61**, 1240 (1992).

⁶T. Inoue, Y. Yamamoto, S. Koyama, S. Suzuki, and Y. Ueda, *Appl. Phys. Lett.* **56**, 1332 (1990).

⁷M. Morita, H. Fukumoto, T. Imura, Y. Osaka, and M. Ichihara, *J. Appl. Phys.* **58**, 2407 (1985).

⁸R. Ramesh, H. Gilchrist, T. Sands, V. G. Keramidas, R. Haakenaasen, and D. K. Fork, *Appl. Phys. Lett.* **63**, 3592 (1993).

⁹M. Ishida, I. Katakabe, T. Nakamura, and N. Ohtake, *Appl. Phys. Lett.* **52**, 1326 (1988).

¹⁰G. Apostolopoulos, G. Vellianitis, A. Dimoulas, M. Alexe, R. Scholz, M. Fanciulli, D. T. Dekadjevi, and C. Wiemer, *Appl. Phys. Lett.* **81**, 3549 (2002).

¹¹M. Mullenborn, K. Matney, M. S. Goorsky, N. M. Haegel, and S. M. Vernon, *J. Appl. Phys.* **75**, 2418 (1994).

¹²W. Xie, D. C. Grillo, R. L. Gunshor, M. Kobayashi, H. Jeon, J. Ding, A. V. Nurmikko, G. C. Hua, and N. Otsuka, *Appl. Phys. Lett.* **60**, 1999 (1992).

¹³L. V. Goncharova, D. G. Starodub, E. Garfunkel, T. Gustafsson, V. Vaithyanathan, J. Lettieri, and D. G. Schlom, *J. Appl. Phys.* **100**, 014912 (2006).

¹⁴M. Schreck, H. Roll, and B. Stritzker, *Appl. Phys. Lett.* **74**, 650 (1999).

¹⁵F. Hörmann, H. Roll, M. Schreck, and B. Stritzker, *Diamond Relat. Mater.* **9**, 256 (2000).

¹⁶J. Delgado, F. Sanchez, R. Aguiar, Y. Maniette, C. Ferrater, and M. Varela, *Appl. Phys. Lett.* **68**, 1048 (1996).

¹⁷S. Gsell, T. Bauer, J. Goldfuß, M. Schreck, and B. Stritzker, *Appl. Phys. Lett.* **84**, 4541 (2004).

¹⁸G. M. Prinz, A. Reiser, T. Röder, M. Schirra, M. Feneberg, U. Röder, R. Sauer, K. Thonke, S. Gsell, M. Schreck, and B. Stritzker, *Appl. Phys. Lett.* **90**, 233115 (2007).

¹⁹T. Wagner, G. Richter, and M. Rühle, *J. Appl. Phys.* **89**, 2606 (2001).

²⁰L. Ickert and H. G. Schneider, *Wachstum Einkristalliner Schichten* (VEB Deutscher Verlag für Grundstoffindustrie, Leipzig, 1983), p. 141.

²¹K.-H. Thürer, M. Schreck, and B. Stritzker, *Phys. Rev. B* **57**, 15454 (1998).